Contribution from the Department of Chemistry,
Simon Fraser University, Burnaby, British Columbia, Canada V5A 1S6

# Large Sn-E-Sn (E = Te, Se, S) Angles: Tri-*tert*-butylstannyl Chalcogenides

R. J. Batchelor, F. W. B. Einstein,* C. H. W. Jones,* and R. D. Sharma

*Received April 19, 1988*

The X-ray crystal structures of the isomorphous compounds $(((CH_3)_3C)_3Sn)_2E$, where E = Te, Se, S, are reported with the following respective crystal data: space group $C2/c$, $Z = 4$; $R_F = 0.034$, 0.033, 0.028 for 2147, 1409, and 2568 observed data; fw = 707.67, 659.03, 612.13; $T = -45$, 23, 23 °C; $a = 8.830$ (5), 8.8975 (18), 8.8869 (11) Å; $b = 15.742$ (7), 15.996 (5), 16.018 (2) Å; $c = 22.297$ (2), 21.9080 (15), 21.733 (3) Å; $\beta = 90.18$ (3), 89.743 (11), 89.788 (11)°; $V = 3099$, 3118, 3094 Å$^3$. The repulsions arising from the bulky substituents lead to unusually large anisotropic thermal motion of the chalcogen and also to expanded Sn-E-Sn angles: 122.26 (7)° (Te), 127.4 (2)° (Se), 134.2 (2)° (S). Our results can be rationalized in terms of "bent" Sn-E bonds.

## Introduction

The structures of molecules in the series $(R_3M)_2E$ (E = O, S, Se, Te; M = Si, Ge, Sn; R = benzyl (Bz), phenyl (Ph), *tert*-butyl (tBu)) have been studied[1-12] with a view to identifying the electronic and steric factors that determine the M-E-M bond angle. Simple VSEPR theory predicts such species to be bent at E as a consequence of the stereochemical influence of the chalcogen nonbonding valence electron pairs. For some oxides however $((Bz_3Sn)_2O$,[2] $(Bz_3Ge)_2O$,[3] $(Ph_3Si)_2O$,[4] and $(tBu_3Sn)_2O$[1]) the bond angle at oxygen is 180°. The possibility of this linearity being a result of $p\pi$-$d\pi$ bonding between O and M has been disputed for neutral species of this type.[12] An alternative explanation based on the second-order Jahn-Teller effect has been put forward.[5] In this model the formally nonbonding electron pairs on O are effectively stereochemically inert toward substituents whose valence electrons are much less tightly bound.

It is well-known, for main-group hydrides possessing nonbonding valence electron pairs, that the H-E-H bond angles rapidly approach 90° upon descending the group (e.g.: $H_2O$, 104.5°; $H_2S$, 92.1°; $H_2Se$, 91°; $H_2Te$, 90°), implying a larger stereochemical influence for the lone pairs of the chalcogens (S, Se, Te). The Jahn-Teller model indicates that linearity at the divalent chalcogens is likely to occur only with anionic substituents.[6] Consequently, the neutral molecules $(R_3M)_2E$ are found to be bent when E is S[1,6-9] Se,[10] or Te.[11] For the species $(R_3Sn)_2E$ (E = S, Se, Te), Sn-E-Sn angles in the range 103.4° $((Ph_3Sn)_2Se)$[10] to 107.4° $((Ph_3Sn)_2S)$[6] have been observed previously. Presumably these angles represent the lower limits permitted by steric interactions between the two $SnR_3$ groups.

The present study was carried out in the interest of probing the steric influence of bulkier ligands on the bond angle at the chalcogen.

## Experimental Section

Crystals of $(((CH_3)_3C)_3Sn)_2E$,[13] where E = Te (**1**) and Se (**2**), were grown from degassed pentane/ethanol solutions by controlled solvent evaporation in a two-part, evacuated, sealed vessel. Crystals of $(((CH_3)_3C)_3Sn)_2S$ (**3**) crystallized from a similar solution by evaporation in air. The crystals were mounted on Pyrex filaments by using 5-min epoxy resin. In the case of **1** the crystal was thinly coated with epoxy to prevent air oxidation. **2**, which is also slowly oxidized in air (noticeable colorization of the crystals after 2-week exposure to air), was deemed stable enough to forgo this treatment.

**Table I.** Crystallographic Data for $(((CH_3)_3C)_3Sn)_2E$, Where E = Te (**1**), Se (**2**), or S (**3**)

| compd | **1** | **2** | **3** |
|---|---|---|---|
| formula | $C_{24}H_{54}Sn_2Te$ | $C_{24}H_{54}Sn_2Se$ | $C_{24}H_{54}Sn_2S$ |
| cryst syst | monoclinic | monoclinic | monoclinic |
| space group | $C2/c$ (No. 15) | $C2/c$ (No. 15) | $C2/c$ (No. 15) |
| $a$, Å | 8.830 (5) | 8.8975 (18) | 8.8869 (11) |
| $b$, Å | 15.742 (7) | 15.996 (5) | 16.018 (2) |
| $c$, Å | 22.297 (2) | 21.9080 (15) | 21.733 (3) |
| $\beta$, deg | 90.18 (3) | 89.743 (11) | 89.788 (11) |
| $V$, Å$^3$ | 3099 | 3118 | 3094 |
| temp, °C | −45 | 23 | 23 |
| $Z$ | 4 | 4 | 4 |
| fw | 707.67 | 659.03 | 612.13 |
| $\rho_c$, g cm$^{-3}$ | 1.517 | 1.404 | 1.314 |
| $\mu$(Mo K$\alpha$), cm$^{-1}$ | 25.51 | 27.72 | 16.93 |
| $\lambda$, Å | 0.71069 | 0.71069 | 0.71069 |
| transmission | 0.534-0.636 | 0.549-0.753 | 0.572-0.615 |
| min-max $2\theta$, deg | 2-50 | 2-45 | 2-55 |
| $R_F$[a] | 0.034 | 0.033 | 0.028 |
| $R_{wF}$[b] | 0.041 | 0.042 | 0.031 |

[a] $R_F = \sum(|F_o| - |F_c|)/\sum|F_o|$, for $F_o \geq 5\sigma(F_o)$. [b] $R_{wF} = [\sum(w(|F_o| - |F_c|)^2/\sum(wF_o^2)]^{1/2}$, for $F_o \geq 5\sigma(F_o)$.

An Enraf-Nonius CAD-4F diffractometer, equipped with an extensively modified low-temperature attachment and using graphite-monochromatized radiation, was used for data collection. The unit cell and diffraction data for **1** were measured at −45 °C. Crystals cooled to lower temperatures undergo a completely reversible transition at −55 °C, which results in a splitting of the diffraction maxima into two equal-intensity components. The separation of the two components ($\omega$-$2\theta$ scans) increases as the temperature is lowered further. When the crystal is rewarmed above −55 °C, these merge again and show no loss in intensity. The data for both **2** and **3** were recorded at room temperature. Crystals of **2** fracture irreversibly upon slow cooling to −45 °C and those of **3** at −10 °C.

The unit cell of **1** was determined from 22 reflections at $\theta$ 14-23°, that of **2** from 23 reflections at $\theta$ 13-19°, and that of **3** from 25 reflections at $\theta$ 22-25°. Two intensity standards were measured every 1 h (**1**) and every 1.5 h (**2**, **3**) of acquisition time. These showed no significant deviations in the case of **1**, while those of **2** and **3** showed a systematic decline in intensity by 8% and 3%, respectively, during the course of data acquisition. Crystallographic data are summarized in Table I. Nonconventional monoclinic unit cells ($\beta < 90°$) are reported for **2** and **3** in order to emphasize the isomorphous nature of the three structures and enable a one-to-one comparison of all structural parameters.

The data were corrected analytically for absorption[14] in each case. Data reduction was performed, including intensity scaling and Lorentz and polarization corrections. The Laue symmetry and systematic absences indicated the space group $C2/c$ or $Cc$. The positions of the Sn (and Te in **1**) atoms were determined ($C2/c$) from the Patterson maps, and the remaining non-hydrogen atoms were found from a subsequent Fourier synthesis.

After isotropic refinement of each structure, electron density difference syntheses followed by anisotropic refinement of the heavy atoms revealed unusually extreme anisotropic motions of the chalcogen atoms, which occur on the crystallographic 2-fold axis (0, $y$, $^1/_4$). This extreme motion could be better described by a split-atom model, involving fractionally occupied sites, one on the 2-fold axis and two general sites, giving rise

(1) Kerschl, S.; Wrackmeyer, B.; Mannig, D.; Nöth, H.; Staudigl, R. *Z. Naturforsch.* **1987**, *42B*, 387.
(2) Glidewell, C.; Liles, D. C. *Acta Crystallogr.* **1979**, *B35*, 1689.
(3) Glidewell, C.; Liles, D. C. *J. Organomet. Chem.* **1979**, *174*, 275.
(4) Glidewell, C.; Liles, D. C. *Acta Crystallogr.* **1978**, *B34*, 124.
(5) Glidewell, C.; Liles, D. C. *J. Organomet. Chem.* **1978**, *159*, 23.
(6) Glidewell, C.; Liles, D. C. *J. Organomet. Chem.* **1981**, *224*, 237.
(7) Krebs, B.; Korte, H.-J. *J. Organomet. Chem.* **1979**, *179*, 13.
(8) Glidewell, C.; Liles, D. C. *Acta Crystallogr.* **1982**, *B38*, 1320.
(9) Wojnowski, W.; Peters, K.; Peters, E.-M.; von Schnering, H. G. *Z. Anorg. Allg. Chem.* **1985**, *525*, 121.
(10) Krebs, B.; Jacobsen, H.-J. *J. Organomet. Chem.* **1979**, *178*, 301.
(11) Einstein, F. W. B.; Jones, C. H. W.; Jones, T.; Sharma, R. D. *Can. J. Chem.* **1983**, *61*, 2611.
(12) Glidewell, C.; Liles, D. C. *Acta Crystallogr.* **1978**, *B34*, 1693.
(13) Gay, I. D.; et al., unpublished results.
(14) DeMeulenaer, J.; Tompa, H. *Acta Crystallogr.* **1965**, *19*, 1014.

0020-1669/88/1327-4636$01.50/0 

**Table II.** Fractional Coordinates (×10⁴) and Equivalent Isotropic Temperature Factors (Å² × 10⁴) for the Non-Hydrogen Atoms of **1** at −45 °C

| atom | *x/a* | *g/b* | *z/c* | *U*(iso) |
|---|---|---|---|---|
| Sn(1) | 1105.4 (5) | 1485.5 (3) | 1507.5 (2) | 411 |
| Te(1)[a] | 0 | 637 (1) | 2500 | 374 (3) |
| Te(11)[b] | 513 (10) | 680 (3) | 2542 (1) | 374 (3) |
| Te(111)[c] | 1152 (15) | 955 (8) | 2619 (5) | 374 (3) |
| C(1) | 2842 (9) | 561 (5) | 1237 (4) | 635 |
| C(2) | −804 (9) | 1514 (6) | 863 (3) | 625 |
| C(3) | 2169 (9) | 2731 (5) | 1661 (4) | 652 |
| C(11) | 2179 (11) | −338 (6) | 1232 (5) | 853 |
| C(12) | 4138 (10) | 589 (6) | 1690 (5) | 802 |
| C(13) | 3438 (12) | 761 (8) | 613 (5) | 999 |
| C(21) | −2097 (9) | 2030 (7) | 1119 (4) | 767 |
| C(22) | −268 (13) | 1891 (10) | 276 (4) | 1049 |
| C(23) | −1347 (12) | 618 (8) | 747 (5) | 1062 |
| C(31) | 1037 (12) | 3416 (6) | 1682 (7) | 1072 |
| C(32) | 3383 (14) | 2889 (7) | 1224 (7) | 1225 |
| C(33) | 2929 (14) | 2740 (7) | 2280 (6) | 1118 |

[a] Site occupancy 0.2654 (17), multiplicity 2. [b] Site occupancy 0.1904 (22). [c] Site occupancy 0.0442 (11).

**Table III.** Fractional Coordinates (×10⁴) and Equivalent Isotropic Temperature Factors (Å² × 10⁴) for the Non-Hydrogen Atoms of **2**

| atom | *x/a* | *y/b* | *z/c* | *U*(iso) |
|---|---|---|---|---|
| Sn(1) | 959.4 (6) | 1494.9 (3) | 1535.9 (3) | 566 |
| Se(1)[a] | 0 | 792 (3) | 2500 | 586 (7) |
| Se(11)[b] | 684 (12) | 890 (5) | 2568 (2) | 586 (7) |
| Se(111)[c] | 1230 (17) | 1209 (11) | 2635 (5) | 586 (7) |
| C(1) | 2597 (12) | 497 (7) | 1304 (6) | 1000 |
| C(2) | −993 (10) | 1477 (7) | 918 (4) | 860 |
| C(3) | 2065 (10) | 2710 (6) | 1588 (5) | 774 |
| C(11) | 1826 (17) | −337 (8) | 1348 (8) | 1525 |
| C(12) | 3864 (14) | 537 (8) | 1761 (7) | 1270 |
| C(13) | 3217 (16) | 618 (10) | 671 (7) | 1501 |
| C(21) | −2178 (12) | 2081 (9) | 1131 (6) | 1259 |
| C(22) | −494 (16) | 1679 (10) | 278 (5) | 1415 |
| C(23) | −1646 (16) | 608 (9) | 917 (8) | 1608 |
| C(31) | 1018 (16) | 3397 (7) | 1664 (10) | 1574 |
| C(32) | 3028 (21) | 2839 (10) | 1052 (7) | 1648 |
| C(33) | 3064 (19) | 2761 (9) | 2124 (8) | 1714 |

[a] Site occupancy 0.182 (4), multiplicity 2. [b] Site occupancy 0.235 (4). [c] Site occupancy 0.083 (3).

to a total of five components for each whole chalcogen atom. The fractional occupancies and positions of these sites and a single isotropic temperature factor for them were refined. The total of the occupancies for the sites was constrained to 1. An attempt to refine an ordered model in the space group *Cc*, in the case of **1**, proved unsuccessful, though this model might be applicable in the apparent reversible "twinning" of the crystal below −55 °C.

Final full-matrix, least-squares refinement included positional coordinates and justified anisotropic temperature factors for all tin and carbon atoms, positional coordinates, fractional occupancies, and a single isotropic temperature factor for the chalcogen, and positional coordinates and a single isotropic temperature factor for the hydrogen atoms, which were placed initially in calculated positions and refined subject to restraints limiting movement within each $CCH_3$ group to rotation about the C–C vector. In the case of **3**, a refined extinction parameter[15] was also included. Weighting schemes were applied such that $\langle w(|F_o| - |F_c|)^2 \rangle$ was near constant as a function of both $|F_o|$ and $(\sin\theta)/\lambda$.[16] The refinements proceeded to convergence.[17] The final positional and equivalent isotropic thermal parameters for the non-hydrogen atoms are given in Tables II–IV for **1**–**3**, respectively. The coordinates and temperature factors for the hydrogen atoms, as well as the anisotropic temperature factors for the non-hydrogen atoms and lists of observed and calculated structure factors for the three structures, are deposited as supplementary material.

(15) Larson, A. C. *Crystallographic Computing*; Munksgaard: Copenhagen, 1970; p 291. $g = 9.1\ (11) \times 10^{-8}$.

(16) **1**: $w = 1$, $|F_o| \le 80$; $w^{1/2} = 80/|F_o|$, $|F_o| > 80$. **2**: $w = [1.65694(t_0(x)) + 1.60275(t_1(x)) + 0.48447(t_2(x))]^{-1}$, where $x = |F_o|/F_{max}$ and $t_n$ are the polynomial functions of the Chebyshev series (Carruthers, J. R.; Watkin, D. J. *Acta Crystallogr.* **1979**, *A35*, 698). **3**: $w = 1$, $|F_o| \le 100$; $w^{1/2} = 100/|F_o|$, $|F_o| > 100$. GOF = 1.33 (**1**), 1.09 (**2**), 1.04 (**3**); GOF = $[\Sigma w(|F_o| - |F_c|)^2/(\text{degrees of freedom})]^{1/2}$.

(17) Maximum shift/error 0.08, 0.007, and 0.06 and maximum peak in final difference map 0.89 (7), 0.65 (4), and 0.47 (7) e Å$^{-3}$ for **1**–**3**, respectively.

**Table IV.** Fractional Coordinates (×10⁴) and Equivalent Isotropic Temperature Factors (Å² × 10⁴) for the Non-Hydrogen Atoms of **3**

| atom | *x/a* | *y/b* | *z/c* | *U*(iso) |
|---|---|---|---|---|
| Sn(1) | 920.8 (3) | 1496.4 (2) | 1540.9 (1) | 459 |
| S(1)[a] | 0 | 907 (4) | 2500 | 474 (7) |
| S(11)[b] | 591 (8) | 983 (5) | 2559 (2) | 474 (7) |
| S(111)[c] | 1005 (17) | 1258 (10) | 2617 (6) | 474 (7) |
| C(1) | 2530 (6) | 486 (4) | 1338 (3) | 796 |
| C(2) | −1054 (5) | 1461 (4) | 931 (2) | 728 |
| C(3) | 2031 (6) | 2715 (3) | 1570 (3) | 717 |
| C(11) | 1756 (9) | −347 (4) | 1404 (4) | 1222 |
| C(12) | 3813 (8) | 536 (5) | 1796 (4) | 1108 |
| C(13) | 3161 (9) | 567 (5) | 692 (4) | 1215 |
| C(21) | −2223 (7) | 2076 (5) | 1135 (4) | 1112 |
| C(22) | −577 (8) | 1634 (6) | 275 (3) | 1202 |
| C(23) | −1727 (8) | 589 (5) | 947 (4) | 1318 |
| C(31) | 978 (9) | 3391 (4) | 1640 (6) | 1414 |
| C(32) | 2953 (13) | 2827 (6) | 1015 (4) | 1555 |
| C(33) | 3055 (11) | 2785 (5) | 2097 (5) | 1593 |

[a] Site occupancy 0.170 (3), multiplicity 2. [b] Site occupancy 0.242 (4). [c] Site occupancy 0.088 (4).

**Table V.** Selected Bond Distances (Å), Uncorrected and Corrected for Thermal Motion, and Angles (deg) for **1** at −45 °C

| Distances | | | | | |
|---|---|---|---|---|---|
| | uncor | cor | | uncor | cor |
| Sn1)–Te(1) | 2.765 (1) | | Sn(1)–Te(11) | 2.684 (3) | |
| Sn(1)–Te(11)′[a] | 2.857 (3) | | Sn(1)–Te(111) | 2.62 (1) | |
| Sn(1)–Te(111)′ | 2.91 (1) | | Sn(1)–C(1) | 2.200 (7) | 2.235 |
| Sn(1)–C(2) | 2.212 (7) | 2.248 | Sn(1)–C(3) | 2.200 (9) | 2.236 |
| **Angles** | | | | | |
| C(1)–Sn(1)–Te(1) | 98.5 (2) | | C(1)–Sn(1)–Te(11) | 93.5 (3) | |
| C(1)–Sn(1)–Te(11)′ | 105.1 (3) | | C(1)–Sn(1)–Te(111) | 92.3 (3) | |
| C(1)–Sn(1)–Te(111)′ | 118.2 (4) | | C(2)–Sn(1)–Te(1) | 105.0 (2) | |
| C(2)–Sn(1)–Te(11) | 114.7 (3) | | C(2)–Sn(1)–Te(11)′ | 96.2 (3) | |
| C(2)–Sn(1)–Te(111) | 129.2 (4) | | C(2)–Sn(1)–Te(111)′ | 85.3 (3) | |
| C(3)–Sn(1)–Te(1) | 117.2 (2) | | C(3)–Sn(1)–Te(11) | 111.8 (3) | |
| C(3)–Sn(1)–Te(11)′ | 119.6 (2) | | C(3)–Sn(1)–Te(111) | 97.5 (4) | |
| C(3)–Sn(1)–Te(111)′ | 116.3 (3) | | C(2)–Sn(1)–C(1) | 111.4 (3) | |
| C(3)–Sn(1)–C(1) | 109.6 (3) | | C(3)–Sn(1)–C(2) | 114.0 (3) | |
| Sn(1)–Te(1)–Sn(1)′ | 122.26 (7) | | Sn(1)–Te(11)–Sn(1)′ | 121.8 (1) | |
| Sn(1)–Te(111)–Sn(1) | 122.2 (4) | | | | |

[a] The prime indicates symmetry operation $-x, y, {}^1/_2 - z$.

**Table VI.** Selected Bond Distances (Å), Uncorrected and Corrected for Thermal Motion, and Angles (deg) for **2**

| Distances | | | | | |
|---|---|---|---|---|---|
| | uncor | cor | | uncor | cor |
| Sn(1)–Se(1) | 2.537 (2) | | Sn(1)–Se(11) | 2.471 (4) | |
| Sn(1)–Se(11)′[a] | 2.627 (4) | | Sn(1)–Se(111) | 2.46 (1) | |
| Sn(1)–Se(111)′ | 2.70 (1) | | Sn(1)–C(1) | 2.22 (1) | 2.287 |
| Sn(1)–C(2) | 2.208 (9) | 2.266 | Sn(1)–C(3) | 2.181 (9) | 2.225 |
| **Angles** | | | | | |
| C(1)–Sn(1)–Se(1) | 95.2 (4) | | C(1)–Sn(1)–Se(11) | 89.4 (4) | |
| C(1)–Sn(1)–Se(11)′ | 105.6 (4) | | C(1)–Sn(1)–Se(111) | 91.3 (4) | |
| C(1)–Sn(1)–Se(111)′ | 120.3 (5) | | C(2)–Sn(1)–Se(1) | 104.0 (3) | |
| C(2)–Sn(1)–Se(11) | 118.8 (4) | | C(2)–Sn(1)–Se(11)′ | 91.0 (3) | |
| C(2)–Sn(1)–Se(111) | 132.7 (5) | | C(2)–Sn(1)–Se(111)′ | 81.0 (4) | |
| C(3)–Sn(1)–Se(1) | 120.1 (3) | | C(3)–Sn(1)–Se(11) | 110.1 (4) | |
| C(3)–Sn(1)–Se(11)′ | 122.6 (3) | | C(3)–Sn(1)–Se(111) | 93.9 (5) | |
| C(3)–Sn(1)–Se(111)′ | 116.1 (4) | | C(2)–Sn(1)–C(1) | 111.6 (4) | |
| C(3)–Sn(1)–C(1) | 110.9 (4) | | C(3)–Sn(1)–C(2) | 113.6 (4) | |
| Sn(1)–Se(1)–Sn(1)′ | 127.4 (2) | | Sn(1)–Se(11)–Sn(1)′ | 126.3 (2) | |
| Sn(1)–Se(111)–Sn(1)′ | 123.6 (5) | | | | |

[a] The prime indicates symmetry operation $-x, y, {}^1/_2 - z$.

**Table VII.** Selected Bond Distances (Å), Uncorrected and Corrected for Thermal Motion, and Angles (deg) for **3**

| Distances | | | | | |
|---|---|---|---|---|---|
| | uncor | cor | | uncor | cor |
| Sn(1)–S(1) | 2.427 (2) | | Sn(1)–S(11) | 2.377 (5) | |
| Sn(1)–S(11)′[a] | 2.508 (5) | | Sn(1)–S(111) | 2.37 (1) | |
| Sn(1)–S(111)′ | 2.53 (1) | | Sn(1)–C(1) | 2.203 (5) | 2.256 |
| Sn(1)–C(2) | 2.204 (5) | 2.249 | Sn(1)–C(3) | 2.188 (5) | 2.228 |
| **Angles** | | | | | |
| C(1)–Sn(1)–S(1) | 95.9 (2) | | C(1)–Sn(1)–S(11) | 90.5 (2) | |
| C(1)–Sn(1)–S(11)′ | 105.1 (3) | | C(1)–Sn(1)–S(111) | 93.2 (3) | |
| C(1)–Sn(1)–S(111)′ | 118.1 (4) | | C(2)–Sn(1)–S(1) | 103.9 (1) | |
| C(2)–Sn(1)–S(11) | 117.1 (2) | | C(2)–Sn(1)–S(11)′ | 92.0 (2) | |
| C(2)–Sn(1)–S(111) | 128.1 (4) | | C(2)–Sn(1)–S(111)′ | 83.9 (4) | |
| C(3)–Sn(1)–S(1) | 118.2 (2) | | C(3)–Sn(1)–S(11) | 109.6 (2) | |
| C(3)–Sn(1)–S(11)′ | 120.7 (2) | | C(3)–Sn(1)–S(111) | 95.7 (5) | |
| C(3)–Sn(1)–S(111)′ | 114.7 (3) | | C(2)–Sn(1)–C(1) | 112.2 (2) | |
| C(3)–Sn(1)–C(1) | 111.6 (2) | | C(3)–Sn(1)–C(2) | 113.6 (2) | |
| Sn(1)–S(1)–Sn(1)′ | 134.2 (2) | | Sn(1)–S(11)–Sn(1)′ | 132.5 (3) | |
| Sn(1)–S(111)–Sn(1)′ | 131.7 (6) | | | | |

[a] The prime indicates symmetry operation $-x, y, {}^1/_2 - z$.

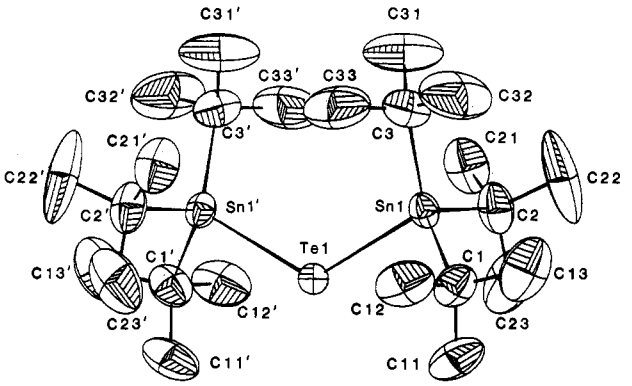


**Figure 1.** Molecular structure of $((tBu)_3Sn)_2Te$ (−45 °C), with H atoms excluded.

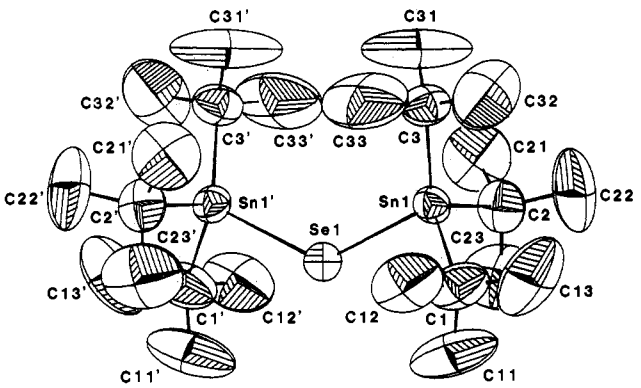


**Figure 2.** Molecular structure of $((tBu)_3Sn)_2Se$, with H atoms excluded.

The programs used for data reduction, structure solution, and initial refinement were from the NRC VAX Crystal Structure System.[18] The program CRYSTALS[19] was employed in the final refinement involving the use of restraints. Complex scattering factors for neutral atoms[20] were used in the calculation of structure factors. Diagrams were generated with the program SNOOPI.[21] All computations were carried out on a MicroVAX-II computer.

(18) Gabe, E. J.; Larson, A. C.; Lee, F. L.; LePage, Y. "NRC VAX Crystal Structure System"; National Research Council: Ottawa, Canada, 1984.
(19) Watkin, D. J.; Carruthers, J. R.; Betteridge, P. W. "CRYSTALS"; Chemical Crystallography Laboratory, University of Oxford: Oxford, England, 1985.
(20) *International Tables for X-ray Crystallography*; Kynoch: Birmingham, England, 1975; Vol. IV, p 99.
(21) Davies, E. K. "SNOOPI Plot Program"; Chemical Crystallography Laboratory, University of Oxford: Oxford, England, 1985.

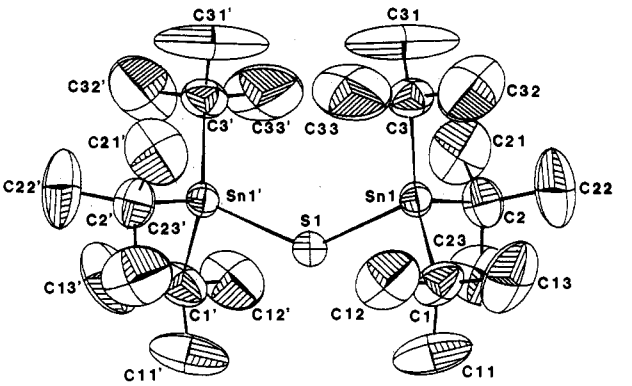


**Figure 3.** Molecular structure of $((tBu)_3Sn)_2S$, with H atoms excluded.

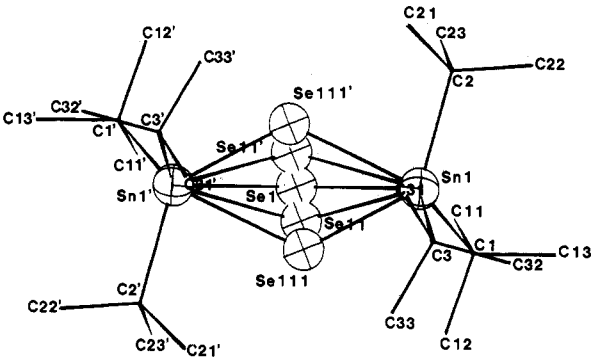


**Figure 4.** Molecule of $((tBu)_3Sn)_2Se$, viewed along [0, 1, 0], with H atoms excluded.

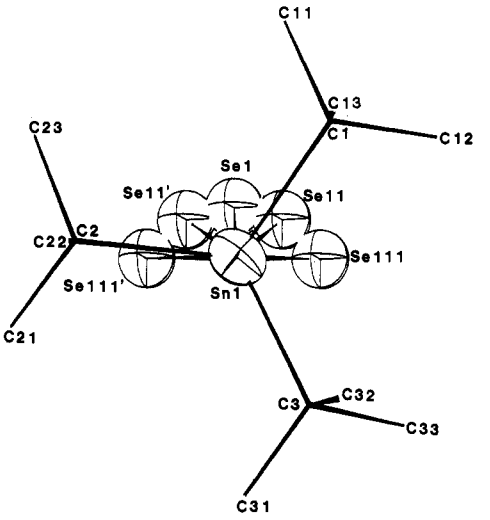


**Figure 5.** $(C_3C)_3SnSe$ fragment of $((tBu)_3Sn)_2Se$, viewed perpendicular to the C(1), C(2), C(3) plane.

The thermal motion was analyzed[22] in terms of a segmented rigid-body model comprising the $Sn(CC_3)_3$ fragment of each molecule. This was treated as three $SnCC_3$ segments hinged at Sn. The weighted residuals for $\Delta U_{ij}$ were 0.075 (**1**), 0.088 (**2**), and 0.055 (**3**). The resulting corrected Sn–C distances are included in the tables of bond distances and angles (Tables V–VII).

## Discussion

The structures of **1–3** are isomorphous. Each molecule is bisected by a crystallographic 2-fold axis passing through the chalcogen atom. Diagrams of the molecules viewed along [1, 0, 0] are shown in Figure 1 (**1**), 2 (**2**), and 3 (**3**). For clarity, only the component of the split chalcogen atom model, described above, that occurs on the 2-fold axis is displayed. The fractionally occupied sites are included in Figures 4 and 5 for **2**. Analogous

(22) Trueblood, K. N. *Acta Crystallogr.* **1978**, *A34*, 950.

views for **1** and **3** are closely similar in terms of the basic geometrical relationships of these sites and the conformation of the molecule as a whole. The selenide diagrams may be taken as representative of the series.

The arrangement of the split-atom sites, discussed below, is consistent with thermal motion of the chalcogen, as opposed to static disorder. The solid-state CP-MAS $^{125}$Te and $^{77}$Se NMR signals for **1** and **2** are unusually weak relative to the $^{119}$Sn and $^{13}$C signals for the same samples as contrasted with the analogous signals for the cyclic compounds $[(tBu)_2SnE]_2$.[13] This implies different relaxation behavior of $^{125}$Te and $^{77}$Se in **1** and **2**, which is consistent with a much larger amplitude of thermal motion for the chalcogens. The possibility that the relative motions of chalcogen and the nearly isotropic tin atoms are exclusively a result of overall molecular rotation about the Sn(1)---Sn(1)′ axis can be ruled out on the basis of the much larger motion of the chalcogen relative to the less anisotropic methyl carbon atoms. Furthermore, Figure 4 shows that the plane containing the arc of the chalcogen motion is not perpendicular to the Sn(1)---Sn(1)′ vector. The angle between the best least-squares plane including E(1), E(11), E(111), E(11)′ and E(111)′ and the plane defined by Sn(1), E(1), and Sn(1)′ is 100.8° (**1**), 97.5° (**2**), and 96.7° (**3**). Examination of Figures 4 and 5 and consideration of closest intramolecular contacts to the chalcogen in each case indicate that this deviation from the perpendicular is steric in nature. That is, as the chalcogen moves from E(1) to E(11) and E(111), it is displaced from the perpendicular plane by C(2)′ and C(21)′ into the space between C(12) and C(33).[23] The asymmetric motion of E with respect to Sn(1) and Sn(1)′ is of interest in that it also results in more acute Sn(1)–E–Sn(1)′ angles (see Tables V–VII).

The relative degrees of chalcogen motion can be inferred from the fractional occupancies of the sites (given in the footnotes to Tables II–IV). The occupancy-weighted average displacement magnitudes from the central position E(1) are 0.28 Å (**1**), 0.52 Å (**2**), and 0.46 Å (**3**). The weighted average angular displacement magnitudes, from E(1) about the midpoint of the Sn(1)---Sn(1)′ vector, are 12° (**1**), 27° (**2**), and 28° (**3**). The lesser motion in the case of tellurium is presumably a consequence of the lower temperature for this structural determination and also the larger moment of inertia of the more massive chalcogen atom. The motions of selenium and sulfur, both at room temperature, are comparable. The larger distance displacement observed for selenium, relative to that of sulfur, is presumably a consequence of the greater distance of Se from the fulcrum point (1.125 Å) compared to that for S (0.944 Å). For the angular displacement, the relative order is reversed.

This type of thermal motion has not been reported previously for structures of $(R_3M)_2E$,[1,6-11] where E = Te, Se, S, M = Sn, Ge, Si, and R = phenyl, benzyl. We take this phenomenon to be one consequence of the expansion of the Sn–E–Sn angle, imposed by the steric bulk of the tri-*tert*-butylstannyl groups. Indeed, the Sn(1)–E(1)–Sn(1)′ angles (122.26 (7)° (**1**), 127.4 (2)° (**2**), 134.2 (2)° (**3**); see Tables V–VII) are by far the largest observed for $(R_3Sn)_2E$ species of the respective chalcogens. By contrast, the values observed in the analogous $(Ph_3Sn)_2E$ (Ph = phenyl) are 103.68 (2)° (E = Te),[11] 104.3° (average; E = Se),[10] and 107.4 (1)° (E = S).[6]

Figure 5 shows the $(C_3C)_3SnSe$ fragment of **2**, including all the 2-fold-related, fractionally occupied selenium sites, viewed in the projection of the plane formed by C(1), C(2), and C(3). From this diagram it is evident that the chalcogen is considerably displaced from the position expected for idealized $sp^3$ hybridization at Sn(1), which, in this view, would have eclipsed Se(1). Such displacement is also observed, but to a smaller degree, in the less hindered structures previously reported $(Bz_3Sn)_2S$[1] and $(Ph_3Sn)_2E$ (E = Te,[11] Se,[10] S[6]). Presumably, this is the primary means of relief of angular strain at the chalcogen atom, given that the known

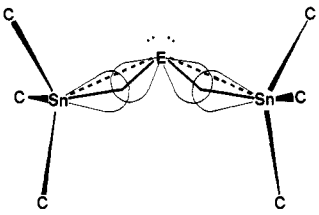


**Figure 6.** Model for sterically imposed bond deformation in $(R_3Sn)_2E$ (E = S, Se, Te).

preference of the divalent chalcogens for bond angles approaching 90° implies the use of pure p-type E orbitals in bonding. The fact that an idealized $sp^3$ hybrid orbital on Sn does not lie along the Sn–E vector suggests that the Sn–E–Sn interatomic angle is not a true indicator of the hybridization of the valence orbitals of E used in Sn–E–Sn bonding. If the region of maximum Sn–E orbital overlap is displaced from the interatomic axis in the Sn–E–Sn plane as shown in Figure 6, then the E hybrid orbitals used in bonding will have more p-orbital character (i.e. the interlobal angle at E is more acute) than the Sn–E–Sn interatomic angle suggests. Such a situation should lower the energy barrier to pendular motion of E about the Sn---Sn axis. In the hypothetical case in which the idealized $sp^3$ atomic orbitals on the two tin atoms are coaxial, as might result with $SnR_3$ groups of even greater steric bulk than $Sn(tBu)_3$, a central atom (E), displaced from the Sn---Sn midpoint in the plane perpendicular to this axis, could move through a 360° arc about the Sn---Sn axis with no change in bonding orbital overlap to the Sn atoms.

For each of the three molecules reported here the calculated idealized trigonal axis of each $SnC_3$ fragment is in the Sn(1), E(1), Sn(1)′ plane. The angle at Sn between this axis and the Sn–E(1) vector is 12.5° (**1**), 16.7° (**2**), and 14.3° (**3**). In each molecule, a point chosen to lie on this idealized axis at a distance of 1 covalent radius (1.41 Å) from Sn toward the molecular center occurs 1.42 Å (**1**), 1.25 Å (**2**), and 1.12 Å (**3**) from E(1). These distances may be compared with the covalent radii of the respective chalcogens, 1.36, 1.16, and 1.02 Å. The angles described at E(1) by these points and their 2-fold-related opposites are 97.5° (**1**), 89.7° (**2**), and 97.9° (**3**). The E(1)–Sn–C bond angles range widely (see Tables V–VII), about "average" values of 109.3° (**1**) and 109.2° (**2** and **3**). The C–Sn–C (Tables V–VII) and Sn–C–C and C–C–C angles[24] display much narrower ranges, remaining closer to the tetrahedral value of 109.5°, consistent with overall $sp^3$ hybridization at Sn. This implies that sterically imposed strain is accommodated largely by the distortion of the Sn–E–Sn linkage. While such geometrical considerations are not, by themselves, sufficient to describe the valence electron distributions about the chalcogen atoms, they support the contention that S, Se, and Te employ nearly pure p orbitals for bonding in these compounds.

All bond lengths in these compounds are consistent with single covalent bonds.[25] The Sn(1)–E(1) bond lengths (Tables V–VII), 2.765 (1) Å, 2.537 (2) Å, and 2.427 (2) Å (**3**), are generally slightly longer than those in the analogous $(Ph_3Sn)_2E$ compounds, 2.7266 (6) Å (E = Te),[11] 2.521 (3)–2.538 (3) Å (E = Se),[10] and 2.370 (4), 2.403 (4) Å (E = S).[6] The Sn(1)---Sn(1)′ distances, 4.843 (1) Å (**1**), 4.549 (1) Å (**2**), and 4.473 (1) Å (**3**), are all larger than twice the Sn van der Waals radius, 4.34 Å. Therefore, a Sn---Sn nonbonded contact does not limit the Sn–E–Sn bond angle.[26] The closest C---C nonbonded contact between the two $tBu_3Sn$ groups of a single molecule is C(21)---C(33)′ in each case (3.81 (2) Å (**1**), 4.05 (2) Å (**2**), 4.07 (2) Å (**3**)). Interestingly, the closest intermolecular C---C separations are shorter than these (C(12)---C(12)″ = 3.76 (2) Å (**1**), 3.72 (2) Å (**2** and **3**).[27] This

(23) The three closest carbon atoms to E(111) in each case are as follows: **1**, C(33) (3.31 (2) Å), C(21)′ (3.38 (2) Å), C(12) (3.41 (2) Å); **2**, C(21)′ (3.16 (2) Å), C(33) (3.17 (3) Å), C(2)′ (3.21 (2) Å); **3**, C(2)′ (3.17 (2) Å), C(21)′ (3.20 (2) Å), C(33) (3.25 (2) Å).

(24) Sn–C–C: **1**, 108.8 (5)–111.6 (6)°; **2**, 108.0 (8)–113.1 (7)°; **3**, 108.5 (4)–112.4 (4)°. C–C–C: **1**, 105.1 (9)–113.2 (9)°; **2**, 104.8 (12)–110.9 (12)°; **3**, 105.3 (7)–110.8 (7)°.

(25) C–C: **1**, 1.47 (1)–1.53 (1) Å [1.51–1.58 Å]; **2**, 1.45 (1)–1.51 (1) Å [1.54–1.60 Å]; **3**, 1.439 (8)–1.519 (8) Å [1.544–1.606 Å]. The numbers in brackets are the ranges of corrected distances after thermal motion analysis.

(26) A hard-atom Sn---Sn contact is suggested to be ≃3.64 Å.[12]

(27) The double prime indicates the symmetry operation $1 - x, y, {}^1/_2 - z$.

suggests that packing forces may have a significant influence on the Sn-E-Sn angle and also indicates how easily this angle is deformed. There are no intermolecular contacts, involving either Sn or the chalcogen atoms, within van der Waals distances.

**Acknowledgment.** F.W.B.E. and C.H.W.J wish to acknowledge that this work was supported by grants from the Natural Sciences and Engineering Research Council of Canada.

**Registry No.** $(((CH_3)_3C)_3Sn)_2Te$, 117680-22-5; $(((CH_3)_3C)_3Sn)_2Se$, 117680-23-6; $(((CH_3)_3C)_3Sn)_2S$, 112164-30-4.

**Supplementary Material Available:** Tables of crystallographic experimental and structure refinement data, hydrogen atom coordinates and temperature factors, anisotropic temperature factors for the non-hydrogen atoms, C-C bond distances, and Sn-C-C and C-C-C bond angles (11 pages); tables of observed and calculated structure factors (64 pages). Ordering information is given on any current masthead page.

Contribution from the Department of Chemistry, The University of Minnesota—Duluth, Duluth, Minnesota 55812

# Spectroscopic and Structural Characterization of the Nine-Coordinate Adduct of Tris(dipivaloylmethanato)europium(III) with 2,2′:6′,2″-Terpyridine

R. C. Holz and L. C. Thompson*

*Received April 21, 1988*

Tris(dipivaloylmethanato)(2,2′:6′,2″-terpyridine)europium(III), [Eu(DPM)$_3$terpy], was synthesized from [Eu(DPM)$_3$] and 2,2′:6′,2″-terpyridine in carbon tetrachloride. The complex was characterized by infrared and luminescence spectroscopy. The infrared spectrum indicated all three nitrogen atoms of the terpyridine ligand were bound to the metal ion. The luminescence spectrum was recorded at 77 K and revealed a broad (15 cm$^{-1}$) unresolvable single transition in the $^5D_0 \rightarrow {}^7F_0$ region. The $^5D_0 \rightarrow {}^7F_1$ region contained six bands and the $^5D_0 \rightarrow {}^7F_2$ region contained nine bands, indicating two distinct emitting metal centers. The luminescence spectrum suggested that the site symmetry of both metal centers is $C_1$. The structure of [Eu(DPM)$_3$terpy] was solved by single-crystal X-ray diffraction methods. The complex was found to crystallize in the monoclinic space group $P2_1/a$ with $a$ = 18.487 (6) Å, $b$ = 28.175 (7) Å, $c$ = 19.434 (10) Å, $\beta$ = 91.57 (3)°, and $V$ = 10 118.8 Å$^3$. Two isomers were found to exist in the unit cell with the ligating atoms forming a nine-coordinate distorted tricapped trigonal prism with each metal center. The two isomers differ by only small variations in bond angles and distances due to steric effects. The average Eu-O and Eu-N bond distances are 2.380 and 2.645 Å for the first Eu(III) ion and 2.385 and 2.663 Å for the second Eu(III) ion. The site symmetry of both metal centers is $C_1$, which is consistent with the luminescence spectrum.

## Introduction

Many lanthanide(III) complexes have been studied extensively because of their highly efficient luminescence and lasing ability.[1] The great majority of these contain oxygen or nitrogen donor ligands, and spectroscopic measurements have been used to determine the symmetry, coordination number, dissociation constants, number of bound water molecules, excited-state lifetimes, metal-metal distances (from energy transfer), number of distinct metal environments, and bonding nature of the ligands.[2]

The lanthanide(III) ion most suited for this type of study is the Eu(III) ion because of its nondegenerate ground ($^7F_0$) and first excited ($^5D_0$) states. Since $J = 0$ for both states, neither level can be split by the crystal field, so any subsequent emission from the excited state to the ground state would result in a single electronic transition for each distinct Eu(III) environment. The other energy levels are degenerate and will be split into the various Stark components depending on the symmetry of the crystal field about the metal center. The electronic transitions that occur among these levels are determined by the selection rules appropriate to the crystal field that is present, and as a result, the symmetry about the metal ion can be deduced.[3]

Since the discovery by Hinckley[4] in 1969 that the lanthanide chelate complex tris(dipivaloylmethanato)europium(III) ([Eu(DPM)$_3$]) acted as an NMR shift reagent, the structural features of adducts of this complex have been of great interest. Several adducts of [Eu(DPM)$_3$] have been synthesized and their properties in the solid and solution states studied.[5,6] Many of these complexes contain neutral nitrogen donor ligands with coordination numbers of 7 or 8. Since the $\beta$-diketone ligand DPM contains large, bulky *tert*-butyl groups, adducts of [Eu(DPM)$_3$] with coordination numbers greater than 8 have never been reported even though other nine-coordinate complexes with $\beta$-diketone ligands have been synthesized, specifically [(facam)$_3$Pr(DMF)$_3$Pr(facam)$_3$][7] (facam = 3-(trifluoroacetyl)-*d*-camphorato), [Eu(TTFA)$_3$terpy][8] (TTFA = thenoyltrifluoroacetonato), and [Eu(DBM)$_3$terpy[8] (DBM = dibenzoylmethanato). The last two complexes contain the neutral nitrogen donor ligand 2,2′:6′,2″-terpyridine. Because terpyridine is a planar ligand with some flexibility, the steric effects between terpyridine and DPM were expected to be small enough to permit complexation. The synthesis of the first nine-coordinate adduct of [Eu(DPM)$_3$] with terpyridine and its characterization by spectroscopic methods and X-ray crystallography are reported here.

## Experimental Section

**Materials.** All the reagents required for this work were used without further purification. Hydrated europium nitrate (99.9%) was purchased from the Research Chemicals Co. Dipivaloylmethane (98%) was purchased from Willow Brook Laboratories, Inc., and 2,2′:6′,2″-terpyridine (98%) was purchased from the Aldrich Chemical Co.

**Preparation of [Eu(DPM)$_3$terpy].** [Eu(DPM)$_3$] was prepared by the method of Eisentraut and Sievers, and the desired product was purified before use by sublimation under vacuum.[9] The title compound was

(1) Thompson, L. C. Complexes. In *Handbook on the Physics and Chemistry of Rare Earths*; Gschneider, K. A., Eyring, L., Eds.; North-Holland: Amsterdam, 1979; pp 211-2.
(2) Horrocks, W. DeW., Jr.; Albin, M. *Prog. Inorg. Chem.* **1984**, *31*, 1-104.
(3) Pradervand, G. O. Luminescence et Structure de Composes de L'Ion Europium(III): Nitrates Doubles et Complexes avec les Ionophores 18-Podand, 18-Couronne-6 et 21-Couronne-7. These de Doctarat, de L'Universite de Lausanne, 1985; p 8.
(4) Hinckley, C. C. *J. Am. Chem. Soc.* **1969**, *91*, 5160-2.
(5) Sievers, R. E., Ed. *Nuclear Magnetic Resonance Shift Reagents*; Academic: New York, 1973; pp 34-5.
(6) Forsberg, J. H. Rare Earth Elements. *Gmelin Handbook of Inorganic Chemistry*; Verlag Chemie: Weinheim, FRG, 1981; Vol. 39, Part D3, pp 136-153.
(7) Cunningham, J. A.; Sievers, R. E. *J. Am. Chem. Soc.* **1975**, *97*, 1586-8.
(8) Melby, L. R.; Rose, N. J.; Abramson, E.; Caris, J. C. *J. Am. Chem. Soc.* **1964**, *86*, 5117-25.
(9) Eisentraut, K. J.; Sievers, R. E. *J. Am. Chem. Soc.* **1965**, *87*, 5254-5.

0020-1669/88/1327-4640$01.50/0 